

Effect of geometry on stress relaxation in InAs/GaAs rectangular nanomesas: Multimillion-atom molecular dynamics simulations

Maxim A. Makeev,^{a)} Rajiv K. Kalia, Aiichiro Nakano, and Priya Vashishta

Collaboratory for Advanced Computing and Simulations, Department of Chemical Engineering, Department of Materials Science and Engineering, Department of Physics and Astronomy, and Department of Computer Science, University of Southern California, Los Angeles, California 90089-0242

Anupam Madhukar

Nanostructure Materials and Devices Laboratory, Department of Materials Science and Engineering, Department of Physics and Astronomy, University of Southern California, Los Angeles, California 90089-0241

(Received 28 February 2005; accepted 7 June 2005; published online 13 December 2005)

We report the results of multimillion-atom parallel molecular dynamics simulations performed to investigate the lattice-misfit-induced stress relaxation in nanometer-sized rectangular GaAs mesas covered with InAs overlayers of 12-ML thickness. The morphology of atomic planes in the InAs overlayers and the stress distributions in the mesas are studied for varied linear dimensions and aspect ratios. We find that the lattice-mismatch-induced stress relaxation pathways is strongly dependent on the mesa and InAs overlayer geometry. The lattice-misfit-associated stress is accommodated through both the morphology changes of the InAs overlayer planes and the stress accommodation in the GaAs mesa interior. The effects are quantified by computing the atomic displacements in the InAs overlayer atomic planes and the hydrostatic stress distributions. Simulation results reveal that, as the aspect ratio of the rectangular mesa top increases, the morphology of the atomic planes shows a transition from dimple-type morphology, characteristic for mesas of square geometry, to semiperiodic modulations of displacement fields accompanied by the overall downward relaxation. The conclusions regarding the stress relaxation mechanism are supported by comparing the topography of the displacement field patterns with those of the hydrostatic stress observed in the mesa systems of different geometries. The obtained results are in qualitative agreement with experiments. © 2005 American Institute of Physics.

[DOI: [10.1063/1.1988970](https://doi.org/10.1063/1.1988970)]

I. INTRODUCTION

The growth of lattice-mismatched overlayers on prepatterned (nonplanar) substrates has been employed as a promising pathway for creating nanometer scale features, such as nanoboxes, nanowires, and truly three-dimensional (3D) coherent islands via molecular beam epitaxy (MBE) and metal-organic chemical vapor deposition (MOCVD) techniques.^{1,2} These techniques allow one to achieve a regular lateral arrangement of nanofeatures, which is not attainable by conventional heteroepitaxy on planar substrates. The ordered superstructures of coherent three-dimensional island quantum dots (QDs), obtained via overgrowth of freestanding islands on planar substrates, are of growing interest due to potential for creating future generations of electronic and optoelectronic devices.¹⁻⁴ The preferential islanding on the nonplanar (patterned) substrates has been experimentally achieved for InAs/GaAs (Refs. 5-10) and Ge/Si systems.¹¹⁻¹³ These works have shown a number of specific features pertaining to these systems, as compared to the conventional heteroepitaxy on planar substrates. It was observed that, in growth on two-dimensional confined mesas, the 3D island formation occurs for large deposition amounts; for InAs/GaAs nanomesas of ≤ 100 -nm sizes, the islanding was suppressed up

to 12 MLs. This is unlike the growth on GaAs planar substrates or long stripe mesas, where the 3D island formation normally takes place as the deposited InAs amount exceeds 1.6 MLs. Furthermore, in the stripe mesa systems, 3D islands are formed with remarkably regular positioning on the mesas tops, when the deposited amount exceeds the critical value for a given geometry. The possibility of preferential formation of highly lattice-mismatched ($\approx 7\%$ mismatch) InAs islands on nanometer-sized GaAs mesas was demonstrated for both square⁵⁻⁷ and stripe^{8,9} mesa geometries. Moreover, Guha *et al.* have shown that, in the growth on patterned substrates, the threshold overlayer thickness for initiation of dislocation networks increased and the density of dislocation decreased strongly, as compared to the case of planar substrates.¹⁴ Similar conclusions for the Ge/Si(001) mesa systems were subsequently drawn in Refs. 11-13, where the authors demonstrated that the deposition of lattice-mismatched ($\approx 4\%$ mismatch) Ge overlayers on Si(001) nanometer scale mesas via MBE leads to preferential islanding on the Si mesa tops.

By now, general understanding exists that the 3D island formation in the heteroepitaxy on planar and nonplanar (mesa) substrates occurs due to the lattice-mismatch stress-induced instability. The realization has prompted an extensive development of theoretical methods, designed to describe the stress and strain fields in such structures.¹⁵ Thus, a

^{a)}Electronic mail: makeev@usc.edu

number of theoretical studies have been recently undertaken with the goal of understanding the stress and strain distributions (and their evolution during deposition), in both the lattice-mismatched coherent islands on planar substrates and in the nanomesa systems, using continuum elasticity theory and atomistic simulations. The latter include the molecular dynamics (MD) method. The systems of mesas, with lateral dimensions ranging from hundreds of nanometers to several microns, of square and stripe shapes, were investigated using the finite element (FE) technique in Refs. 16–19. An isolated “freestanding” Ge island on Si(001) substrate was studied by FE method in Ref. 20. Subsequently, the systems of coherent lattice-mismatched islands of both buried and freestanding types have been studied using both continuum elasticity theory-based analytical models and the FE calculations based on continuum elasticity.²¹ Another approach, widely used to uncover the stress behavior in the nanostructures, is based on atomistic simulations. In Refs. 22–31, freestanding and buried InAs/GaAs and Ge/Si islands of pyramidal geometry were studied using MD simulations. The stress and strain field distributions in Si_xN_y nanopixels have been recently studied using large-scale MD simulations.^{32,33} These studies revealed a highly inhomogeneous nature of the stress distributions in such systems. Atomistic simulation studies of {113}-facetted Ge/Si(001) nanomesas were reported in Ref. 34. It was shown that the continuum elasticity theory (as well as its conventional FE implementations) does not adequately describe the regions located near the finite geometry features.³⁴ molecular dynamics simulations of nanometer scale InAs/GaAs mesas of square geometry have been recently reported in Refs. 35–37. It was shown that the pathways for the lattice-mismatch stress relaxation in such systems vary with the fine specifics of the mesa geometry.^{36,37} Thus, as the lateral mesa size grows, the morphology of the InAs overlayer planes was observed to undergo substantial changes,^{36,37} which is indicative of different mechanisms of stress relaxation operative for different lateral sizes. These changes were accompanied by modifications in the hydrostatic stress behavior, with a tensile stress domain appearing at the mesa center, in the case of large mesas. On the other hand, a purely compressive behavior with relaxation towards the mesa edges was observed in the case of mesas with smaller sizes. Since the studies reported in Refs. 35–37 were performed for square mesas only, the issue of the effect of mesa geometry on the stress relaxation pathway was left beyond the scope of these investigations.

In this paper, we report on a multimillion-atom molecular dynamics simulation study of stress behavior in rectangular InAs/GaAs mesa systems. We consider rectangular GaAs mesas with ⟨100⟩-oriented base and {101} sidewalls, positioned on GaAs(001) substrates of fixed thickness. The mesas with different mesa base (top) aspect ratios and sizes are considered. The effects of mesa geometry on the InAs-overlayer-associated stress relaxation are studied. Our MD simulations are based on reliable interatomic potentials that can successfully describe wide range of physical properties of both InAs and GaAs. Our primary emphasis is on the atomically resolved displacement fields and the mechanical stresses in InAs overlayers and GaAs(001) mesa interior

(substrate). We find that the pathways for the lattice-mismatch-induced stress relaxation may vary dramatically as the rectangular mesa aspect ratio is varied from 1 (square mesa) to 3 (rectangular mesa). In the mesas of rectangular geometry, the InAs overlayer atomic planes demonstrate wavy corrugations, with periodicity along the longer lateral direction. Similar stress patterns are observed in the hydrostatic stress distributions. The stress relaxation patterns are reminiscent of those observed in the systems of dislocated flat InAs overlayers on GaAs.

The remainder of the paper is organized as follows. In Sec. II, we describe the simulation methodology including (Sec. II A) interatomic potential scheme, (Sec. II B) simulation system, and (Sec. II C) the methodology of stress calculations. In Sec. III, we present simulation results, concentrating primarily on the morphologies of atomic planes in the lattice-mismatched InAs overlayers, for systems with different aspect ratios. Those are compared with the ones reported for infinite flat InAs overlayers on GaAs. Section III B is devoted to discussion of the hydrostatic stress behavior in the mesa systems with different geometries. Finally, in Sec. IV, we summarize our major results.

II. SIMULATION METHODOLOGY

A. InAs and GaAs interatomic potentials

The interatomic potential scheme, used in this work, has been previously described in the literature.^{37,38} The interatomic potentials for both GaAs and InAs consist of two-body and three-body terms

$$V = \sum_{i < j} V_{ij}^{(2)}(r_{ij}) + \sum_{i, j < k} V_{jik}^{(3)}(\mathbf{r}_{ij}, \mathbf{r}_{ik}), \quad (1)$$

where $r_{ij} = |\mathbf{r}_{ij}|$, $|\mathbf{r}_{ij}| = |\mathbf{r}_i - \mathbf{r}_j|$, and \mathbf{r}_i is the position of the i th atom.

The functional form of the two-body terms, which account for the steric repulsion, Coulomb interaction due to charge transfer, dipole-dipole interaction arising due to large polarizability of negative ions, and van der Waals dipole-dipole interactions, is

$$V_{ij}^{(2)}(r_{ij}) = \frac{H_{ij}}{r_{ij}^n} + \frac{Z_i Z_j}{r_{ij}} e^{-r_{ij}/a} - \frac{D_{ij}}{r_{ij}^4} e^{-r_{ij}/b} - \frac{W_{ij}}{r_{ij}^6}. \quad (2)$$

The three-body terms describe the effects of covalent bond bending and bond stretching, and are given by the following form:

$$V_{jik}^{(3)}(\mathbf{r}_{ij}, \mathbf{r}_{ik}) = B_{jik} \exp\left(\frac{\gamma}{r_{ij} - r_o} + \frac{\gamma}{r_{ik} - r_o}\right) \times \frac{(\cos \theta_{jik} - \cos \bar{\theta}_{jik})^2}{1 + C(\cos \theta_{jik} - \cos \bar{\theta}_{jik})^2} \times \Theta(r_o - r_{ij}) \Theta(r_o - r_{ik}), \quad (3)$$

where $\Theta(x)$ is the Heaviside step function and $\theta_{jik} = (\mathbf{r}_{ij} \cdot \mathbf{r}_{ik}) / (|\mathbf{r}_{ij}| |\mathbf{r}_{ik}|)$.

The parameters of the interatomic potentials for both InAs and GaAs are chosen to closely reproduce the experimental data for lattice constants, cohesive energies, elastic

constants, and surface energies. It was determined that high-pressure structural transitions, phonon density of states, and neutron-scattering data for amorphous phases of the corresponding materials are in good agreement with experiments and the first-principles electronic structure calculations.^{38–42} It should also be noted that the above potential scheme was found to account well for the surface-induced relaxation effects, which have been compared with the first-principles electronic structure calculation results.³⁷

In the problem of heteroepitaxial systems, involving bi-materials, interfaces between the two constituent materials have to be adequately treated in the atomistic simulation. Within the framework of our interatomic potential scheme, InAs–GaAs interfaces are dealt with by employing an environment-dependent interpolation approach, which allows us to describe adequately the InGaAs alloys (with different constituent compositions) as well as the interfaces.³⁷ Further details of the potential scheme are as follows. The two-body interactions between different cations (Ga and In) are approximated by arithmetic averages of the cation-cation interaction potentials, as they appear in the bulk crystalline compounds (GaAs and InAs),

$$V_{\text{Ga-In}}^{(2)}(r) = [V_{\text{Ga-Ga}}^{(2)}(r) + V_{\text{In-In}}^{(2)}(r)]/2. \quad (4)$$

The two-body interaction potential between As (GaAs)–As (InAs) is also linearly interpolated between the potentials for the pure compounds. If an As atom is labeled as $As_{n/4}$ ($n = 0, \dots, 4$), where n is the number of In atoms around the As atom, the As–As interaction potential is then approximated by

$$V_{\text{As}_x\text{-As}_y}^{(2)}(r) = \frac{2-x-y}{2} V_{\text{As}_0\text{-As}_0}^{(2)}(r) + \frac{x+y}{2} V_{\text{As}_1\text{-As}_1}^{(2)}(r), \quad (5)$$

where $x = n/4$, and As_0 and As_1 correspond to atoms with purely Ga and purely In neighbors, respectively. The three-body interaction potential for Ga–As–In triplet is computed as the arithmetic average of the three-body interactions in the pure compounds,

$$V_{\text{Ga-As-In}}^{(3)}(\mathbf{r}_{ij}, \mathbf{r}_{ik}) = [V_{\text{Ga-As-Ga}}^{(3)}(\mathbf{r}_{ij}, \mathbf{r}_{ik}) + V_{\text{In-As-In}}^{(3)}(\mathbf{r}_{ij}, \mathbf{r}_{ik})]/2. \quad (6)$$

The parameters of the interatomic potentials for both InAs and GaAs are given in Ref. 37. Furthermore, in Ref. 37, the implementation of the surface (subsurface)-potential scheme is discussed, and critically compared with available experimental data and the first-principles electronic structure calculations. In general, the interatomic potentials [Eqs. (1)–(6)] provide a good description of the bulk properties of crystalline InAs and GaAs. Moreover, the properties of InGaAs alloys are also reproduced well using these potentials.³⁸

B. Simulated system

The present study is designed to compliment the previously reported investigations of pyramidal InAs/GaAs mesas with square mesa (overlayer) top geometry by Su *et al.*^{35–37} We concentrate primarily on the effects of the mesa geometry on the lattice-misfit-induced stress relaxation in the system, by comparing overall pictures of the stress relaxation in

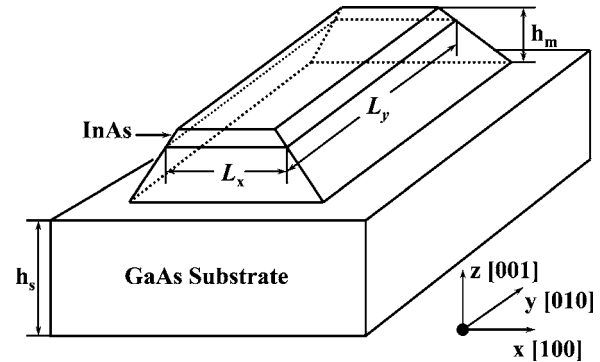


FIG. 1. Schematic of the InAs/GaAs nanomesa with $\langle 100 \rangle$ -oriented rectangular base and $\{101\}$ sidewalls on a GaAs $\langle 001 \rangle$ substrate.

the systems with different rectangular mesas top aspect ratios, varying from 1 (square mesa, as previously reported in Refs. 35–37) to 4 (rectangular mesa). A schematic of the simulated system is shown in Fig. 1. A rectangular base GaAs mesa is positioned on GaAs substrate of fixed height $h_s = 60$ MLs. The GaAs mesa height is kept fixed at $h_m = 50$ MLs in all cases. The lateral dimensions of the GaAs substrate are varied to accommodate different mesas, with mesa top lateral sizes of L_x and L_y . The lateral dimensions of the mesa tops and the number of atoms are given in Table I. In all cases, the mesa has $\langle 100 \rangle$ -oriented rectangular base (see Fig. 1) and $\{101\}$ -oriented sidewalls. Note that, previously, simulation results for square mesas with top lateral sizes of 124.3 and 407.0 Å were reported (see Refs. 35–37). Below, we compare these results with the data for mesa systems with aspect ratios varying from 1.5 to 4 (see Table I). The initial configuration is set up as follows. Initially, all the atoms are placed in the perfect crystalline GaAs bulk positions. Periodic boundary conditions are applied to the GaAs substrate in both x and y directions. The total number of atoms in the simulation cell ranges from ~ 3.2 to $\sim 32.4 \times 10^6$. The computations are performed on a 256-processor Linux cluster at the Collaboratory for Advanced Computing and Simulations. To implement the parallel computations, a spatial decomposition of the systems was performed and the message-passing interface was used. The equations of motion are integrated using a reversible symplectic algorithm,⁴³ with a time step Δt of 2.0 fs. To equilibrate the system and bring the surface and interface atoms in equilibrium positions, MD schedule of 60 000 steps or larger is followed. The equilibrium configuration is obtained as follows. First, the system is quenched to 0 K for $10\Delta t$. Subsequently, we scale the velocities with a factor of 0.8, whenever the temperature of the system is higher than 3 K, every $5\Delta t$ for 5000. The total number of steps used in relaxation is not less than 60 000 steps, depending on the size of the system and the convergence of the stress tensor elements. All the relevant quantities, such as atomic displacements, partial distribution functions, and hydrostatic stresses, are computed for the resulting relaxed configurations.

C. Stress computations

The method for atomically resolved stress tensor computation has been discussed in the literature in sufficient

TABLE I. The InAs/GaAs rectangular mesa sizes in the lateral $x(L_x)$ and $y(L_y)$ directions in angstroms. We assign ID to each mesa dependent on its size (letter) and aspect ratio (number). Letter A is assigned to the smallest mesa with a given aspect ratio, B for the intermediate, and C for the largest. The numbers correspond to the aspect ratio as follows from the data in the table. In each considered case, the mesa has $\langle 110 \rangle$ -oriented base (see Fig. 1) and $\{101\}$ -oriented sidewalls. In the table, N_{atoms} is the number of atoms, and L_y/L_x is the aspect ratio of the rectangular mesa.

| Mesa size/mesa ID | A15 | B15 | C15 | A20 | B20 | C20 |
|--------------------|--------------------|--------------------|---------------------|--------------------|---------------------|---------------------|
| L_x | 124.4 | 305.3 | 407.0 | 124.3 | 309.4 | 407.0 |
| L_y | 192.2 | 463.5 | 621.9 | 248.6 | 618.8 | 814.0 |
| L_y/L_x | 1.5 | 1.5 | 1.5 | 2.0 | 2.0 | 2.0 |
| N_{atoms} | 3.18×10^6 | 6.89×10^6 | 12.61×10^6 | 9.5×10^6 | 12.3×10^6 | 19.2×10^6 |
| Mesa size/mesa ID | A30 | B30 | C30 | A40 | B40 | C40 |
| L_x | 124.4 | 305.2 | 407.0 | 124.4 | 305.3 | 407.0 |
| L_y | 373.1 | 915.8 | 1232.4 | 508.8 | 1232.4 | 1628.1 |
| L_y/L_x | 3.0 | 3.0 | 3.0 | 4.0 | 4.0 | 4.0 |
| N_{atoms} | 4.61×10^6 | 8.97×10^6 | 16.57×10^6 | 5.46×10^6 | 17.58×10^6 | 32.42×10^6 |

details.^{44–46} In this work, we adopt the expression for the stress tensor, which was derived by Cheung and Yip.⁴⁶ The microscopically resolved stress, $\sigma_{\alpha\beta}^i$, associated with an atom i , can be computed via

$$\sigma_{\alpha\beta}^i = \frac{1}{\Omega_i} \left[m_i v_i^\alpha v_i^\beta + \frac{1}{4} \sum_j (r_{ij}^\alpha f_{ij}^\beta + r_{ij}^\beta f_{ij}^\alpha) \right], \quad (7)$$

where $\alpha, \beta \in \{x, y, z\}$, m_i and v_i are the mass and velocity of the atom i , f_{ij}^β is the force acting on atom i due to atom j , r_{ij} is the vector connecting atoms i and j , and Ω_i is the average atomic volume, associated with atom i .^{44–47} The quantity, given by Eq. (7), is then averaged over all atoms residing inside a sphere with a radius of 7.5 Å.

III. STRESS RELAXATION IN THE MESA SYSTEMS

A. Morphologies of InAs overlayer planes

We have investigated the effect of mesa geometry on the stress relaxation in the InAs overlayer atomic planes. Such study can provide important insights into the mechanism of the misfit-induced stress relaxation in the systems with finite geometries. Previously, it was shown that in *square* mesas the pathway for the lattice-misfit-induced stress relaxation depends strongly on the specifics of mesa geometry. On the other hand, only mesa systems with square tops (although with different mesa top sizes) were considered.^{35–37} In this work, we extend the analysis and consider InAs/GaAs mesas with rectangular tops having different aspect ratios. Mesas of rectangular shapes (and, in the limit $L_y/L_x \rightarrow \infty$, stripe mesas) are equally relevant for the experimentally employed systems^{8,9} as the square mesas.^{5–7} Our study allows one to understand how the stress behavior changes with growing aspect ratio and extrapolate the observed behavior to the limit of infinitely long (in the y direction) stripe mesas. By studying the InAs overlayer morphologies, along with the radial distribution functions and the hydrostatic stresses, one can obtain a complete picture of stress behavior in the mesa systems. The observed morphologies of the bottom In plane of the mismatched InAs overlayer, for A20, B20, and C20 mesa systems (see Table I), are shown in Fig. 2. Similar to the previously reported studies (see Refs. 35–37), we con-

centrate on the vertical displacements in the first InAs overlayer plane, which are given in angstroms and are color coded in Fig. 2. As can be seen in Fig. 2, the stress relaxation pathways differ significantly in both the morphology patterns and the magnitude of the atomic displacements for systems with different aspect ratios. The A20 system relaxes similar to the square mesa of the same lateral size (see Ref. 35). The shape of atomic plane's corrugations and the magnitude of atomic displacements in the system also resemble closely the ones observed in the square mesa case. As the lateral size of the rectangular mesa top increases, however, (while keeping the aspect ratio fixed at 2.0), the morphology of the InAs plane changes drastically. In Figs. 2(b) and 2(c), instead of one minimum at the center of the system, observed for the

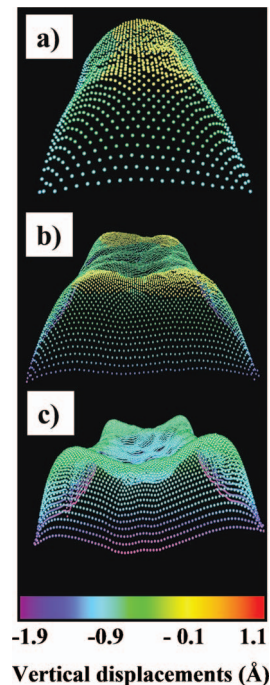


FIG. 2. (Color) Vertical atomic displacements of In atoms in the bottom In atomic plane of the InAs overlayer. Different plots correspond to different mesa geometries: (a) A20, (b) B20, and (c) C20 (see Table I for the notation).

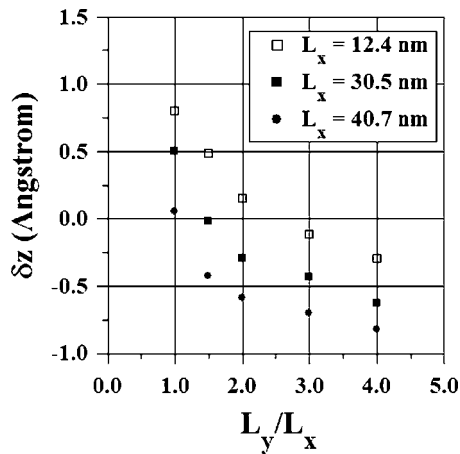


FIG. 3. Maximum displacements in the center of the first In atomic plane of the InAs overlayer are shown as a function of the mesa top aspect ratio, for three InAs/GaAs mesa systems.

largest mesa of square geometry, wavy patterns are observed along the y direction (note that $L_y > L_x$). These wavy patterns can be considered as periodic waves along the $\{110\}$ crystallographic direction. In addition, on the average, large negative displacements in the central region of the plane are observed, showing that the stress relaxation occurs via superimposed overall downward relaxation and wavy morphological corrugations. As one can see in Fig. 2, the three minima of the periodic modulations are confined to the center of the system, i.e., the distance between the first (third) minimum and the mesa edge is larger than the distance between the minima themselves. This raises the issue of the effect of the mesa corners, which act to prevent the downward relaxation. The largest downward displacements (among the mesas with a fixed aspect ratio of $L_y/L_x = 2.0$) are observed for the largest mesa; this observation holds for all investigated mesa aspect ratios. On the other hand, upward displacements observed in the case of rectangular mesas ($L_y > L_x$) are suppressed as compared to the square mesa case. The relaxation proceeds through the formation of wavy modulations and downward displacements. It should be emphasized that periodic patterns have been previously observed in the systems of lattice-mismatched InAs overlayers on the planar GaAs(111) substrates due to dislocation network formation (see discussion below). To further verify the observed picture, we have investigated the mesas with aspect ratios greater than 2 (see Table I, for details). In the case of larger aspect ratios, ripple-type corrugations are also observed. In the case of C30 and C40 mesas, the relaxation occurs already through the formation of the superimposed (in the x and y directions) wavy structures.

To further illustrate the size dependence of the atomic relaxation, Fig. 3 shows the maximum atomic displacement (in angstroms) as a function of the rectangular mesa top aspect ratio. The different symbols in the figure correspond to three different mesa sizes; $L_x = 12.4$, 30.5, and 40.7 nm. As one can see, when the mesa aspect ratio changes from 1 to 4, the magnitude of the maximum displacements drops by more than 200%. Moreover, the upward displacements of large magnitude, observed for square mesas, undergo a transition

and become downward, for mesas with large sizes and aspect ratios. Similar relaxation picture is observed for all studied mesa sizes, which indicates a general character of the observed behavior. The underlying mechanism of the mismatch-induced stress relaxation, leading to such behavior, is defined by the dependence of the critical thickness on the specifics of the mesa geometry and will be discussed below.

The nearly periodic corrugations in the mismatched overlayers, observed in the direction parallel to the shortest mesa side, are not completely unexpected. Indeed, it was demonstrated previously that the overcritical thin InAs films, deposited on GaAs(110) and GaAs(111) substrates, relax the lattice-mismatch-induced strain through the hexagonal dislocation networks, formed at the heterointerfaces. The formation of the dislocation networks leads to the lattice-mismatched overlayer plane modulations, which can be considered as a superposition of nearly periodic waves in the two lateral directions (see, for instance, Refs. 48 and 49). The minima of these modulations are located above the interfacial MD lines. The observed superimposed periodic structure appears to be a natural pathway for stress relaxation, given that the two lateral directions are equivalent to each other for an infinite system (which does not hold for our systems). It can be further argued that, in our case, the development of plane modulation patterns starts to occur as the mesa size grows, approaching the infinite thin film on infinite substrate case. On the other hand, the systems we consider are laterally finite and dislocation-free. They are, however, near the threshold elastic strain, which causes dislocation formation. The energetics of dislocation networks formation was previously investigated in Refs. 48 and 49. The authors reported their results for the period of undulations in the infinite InAs overlayer, deposited on GaAs substrates, as 60 Å, and the maximum magnitude of the periodic undulations ≈ 0.5 Å. The magnitudes of the upward displacements in our case are much larger as compared to the ones observed for the case of infinite substrates (see Fig. 15 of Ref. 48). This is expected since in our case the dislocation network is not developed. It is highly probable that the observed picture constitutes a precursor for the dislocation network formation in our systems. The process of dislocation network formation is defined by a complex interplay between various factors involved. The driving force of the process is defined by the lattice-mismatch-induced stress relaxation pathways, which are system size dependent. On the other hand, the dislocation formation is a thermally activated process and, thus, can be suppressed by lowering the temperature below the activation threshold. While, in some considered cases, the overlayer thickness is larger than the critical for a given geometry, the temperature is kept below the threshold for the formation of the misfit dislocation network. The periodic perturbations are terminated near the mesa corner regions, where the overall relaxation picture is different. In this case, the corner regions are lifted over the average values, with the maximum upward displacement observed in such regions.

To further elucidate the stress relaxation mechanisms in InAs/GaAs mesas, we have computed the partial distribution functions (PDFs) for the mesa systems under consideration

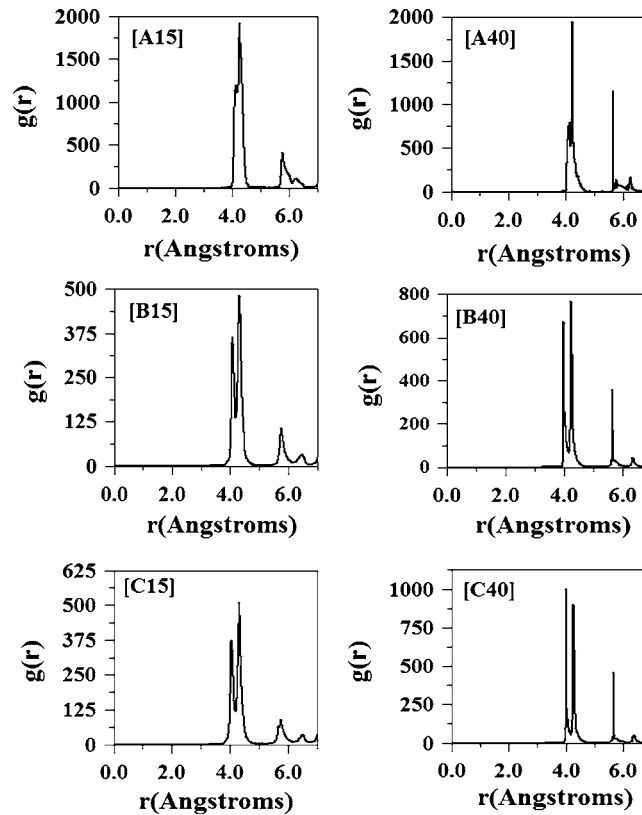


FIG. 4. In-In pair distribution functions for three InAs/GaAs mesa systems with fixed aspect ratios of 1.5 (right column) and 4.0 (left column). The mesa systems are marked according to the specifics of their geometry, as summarized in Table I.

(see Table I). The In-In PDFs for the mesa systems, with aspect ratios of 1.5 (left panel) and 4.0 (right panel), are shown in Fig. 4. First, we concentrate on the behavior of the PDFs for mesas with different top sizes. The general behavior is similar for all aspect ratios, including the square mesa case.^{48,49} Namely, for small size mesas, the InAs overlayer is largely relaxed, with the averaged (over all InAs overlayer atoms) lattice parameter approaching closely the bulk value of the crystalline material. This is consistent with the assumption that the lattice expansion at the GaAs mesa (InAs overlayer) edges allows for substantial relaxation of the misfit-induced strain, but only for mesas of relatively small sizes. As the mesa size increases, the splitting of the first peak is observed, suggesting that the system is not fully relaxed to the InAs bulk value lattice constants. Instead, there are regions, where the lattice constant is being compressed between the GaAs bulk value and that of InAs. The first subpeak position in the PDFs corresponds to ≈ 4.1 Å, and the second subpeak is at ≈ 4.3 Å. The second subpeak intensity increases with the mesa aspect ratio. On the other hand, there is an effective widening of the first peak of the PDF, which takes place with increasing mesa top sizes ratio. The effect is non-negligible even if the aspect ratio was increased only from 1.5 to 2.0. As one can see, the average nearest-neighbor distance widen to cover the interatomic distances corresponding to both compressed and expanded lattices (as compared to the pure InAs and even GaAs crystalline materials). Second important issue to address is the variations in the behavior with the lateral aspect ratio (for fixed mesa sizes). This is similar to the previously observed behavior in

the square nanomesas. Its origin is in the strong lateral correlations in the InAs plane, which does not allow the lateral expansion as compared to the vertical relaxation, which leads to the increase in interatomic distances (as compared to the InAs bulk crystalline value). The effect is strongest for the largest mesa, as expected. The PDFs of the InAs mesa systems with a 4.0 aspect ratios are shown in the right panel of Fig. 4. As one can observe, in this case the qualitative features of the atomic structures (as captured by the PDFs) are similar to those uncovered for the mesas with smaller aspect ratios. One notable feature is observed, though. The second peak of each PDF shows a smaller width, as compared to the 2.0 aspect ratio mesas, while the positions of the peaks remain the same. In general, the behavior of the PDFs suggests that, with growing mesa sizes, the region of highly compressed stresses (strains) appears in the system, due to less freedom to relax as compared to the small mesas. Furthermore, growing aspect ratio prevents the relaxation in one direction (from the two available) and thus serves as a constraint for effective stress relaxation.

B. Hydrostatic stress distributions

The cross-sectional hydrostatic stress distributions (in $x = 0$ plane) are shown in Fig. 5, for the mesas with aspect ratios of 1.5 (upper panel) and 3.0 (lower panel). The hydrostatic stress relaxes differently in the InAs overlayer top region and InAs-GaAs interface region. In the top region, the A15 mesa experiences largest stress relaxation at the mesa center. As L_y increases, the relaxation towards the mesa side-

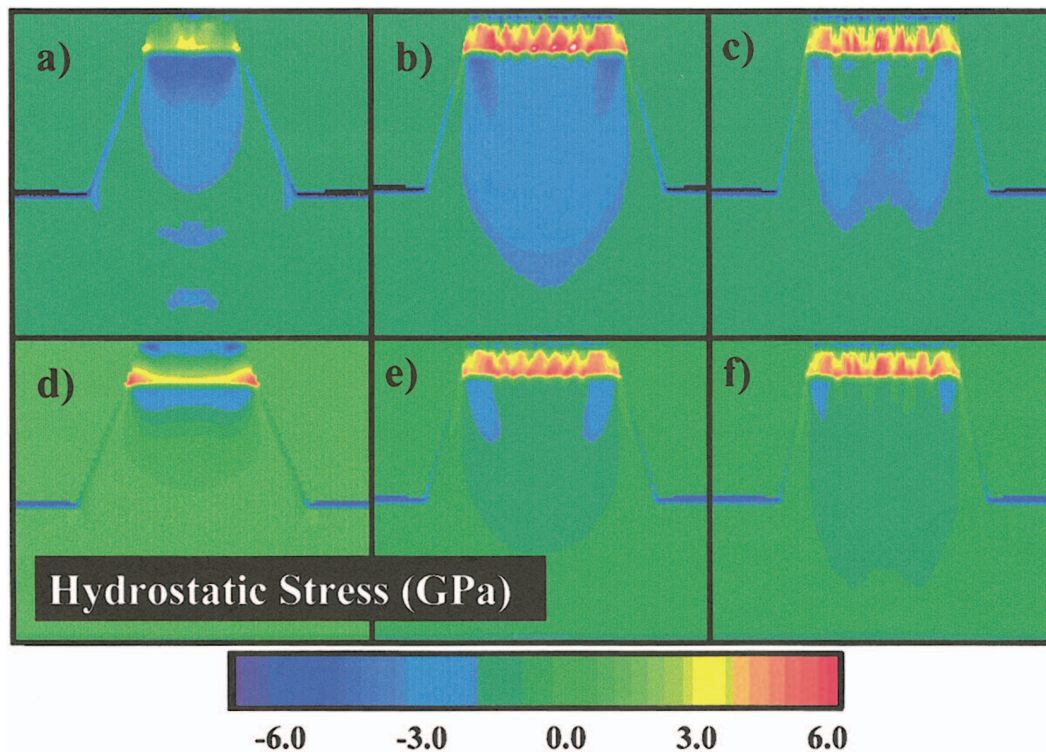


FIG. 5. (Color) The atomically resolved hydrostatic stress distributions, measured in the z - y planes ($x=0$), are shown for six InAs/GaAs mesa systems with different geometries: (a) A15 [$L_x=124.4, L_y/L_x=1.5$]; (b) B15 [$L_x=305.3, L_y/L_x=1.5$]; (c) C15 [$L_x=407.0, L_y/L_x=1.5$]; (d) A30 [$L_x=124.4, L_y/L_x=3.0$]; (e) B30 [$L_x=305.3, L_y/L_x=3.0$]; and (f) C30 [$L_x=407.0, L_y/L_x=3.0$].

walls is observed. For small aspect ratios, there is a compressive stress domain near the interfaces with maximum observed near the center. The maximum shifts towards the mesa edges, as the aspect ratio grows. Note that highly compressive stresses, caused by the InAs overlayer, inhomogeneously relax in the InAs overlayer interior exerting large magnitude of tensile stress on the GaAs mesa and substrates. In the case of large mesas, the hydrostatic stress distribution exhibits patterns resembling periodic modulations along the shortest lateral direction, for small mesa sizes or superimposed waves, when size of the mesa is sufficiently large in both lateral directions. The period of such modulations is consistent with the observed period of displacement fields (see above). In the x direction, the maximum compressive stress shifts from the mesa edges to the center, as the mesa size grows at a large aspect ratio (stripe mesa limit). This behavior of the hydrostatic stress has a number of important consequences. For the stripe mesa systems, it was observed experimentally that the island arrangement on the mesa top surface is size dependent. For small mesa sizes (i.e., for lateral dimensions less than 100 nm), one row of islands is formed. As the lateral size increases, however, the number of rows is 2, with each of these rows located in the close vicinity of the mesa edges. In Ref. 9, it was found that after the mesa size grows beyond 200 nm the regular structures of islands disappear, with island positioning being random. This is indicative of the fact that there are two regimes in stress behavior. For mesas with relatively small lateral dimension (less than 30 nm), the relaxed stress region is located near the mesa center. As mesa size grows, a transition occurs with relaxed regions being located near the mesa edges. One of

the important consequences of experimental results is that, for large mesas, a random patterning in top surface morphology should be observed. Thus, one can conclude that there exists a unique characteristic mesa size (for a given geometry), at which a transition between the two regimes takes place. For length scales exceeding this critical length, the stress relaxation does not undergo fundamental changes; the stress relaxes towards the mesa edges and the region of highly compressed stresses at the mesa center is observed. This is expected, since collective rearrangement of material becomes difficult for large lateral dimensions. Note that in our simulations, we observed that the mesa size growth leads to randomization of the InAs overlayer morphology, with the patterns of superimposed wavy structures being randomized for large mesa dimensions. This indicates that, in the morphological phase diagram, we approach the point of stress-induced instability. Indeed, 12-ML InAs overlayer is below the instability threshold, for small mesa sizes, but becomes overcritical for larger lateral mesa sizes (aspect ratios). The construction of the actual morphological phase diagram is, however, an extremely complex problem and is out of the scope of this paper.

IV. SUMMARY

In summary, we have performed large-scale parallel MD simulations of InAs/GaAs rectangular mesas of nanometer scale with $\{101\}$ -type sidewalls and compared the obtained results with those for square mesas having the same facet orientation. We found that the lattice-mismatch-induced stress relaxation is strongly dependent on the specifics of the

mesa geometry. While, in the case of square mesas of relatively small sizes, the stress relaxation occurs through the corrugation of InAs atomic planes in the form of dome or dimple, the relaxation in the rectangular mesas with high aspect ratios may take place through the formation of periodically modulated atomic plane geometries, which appear as a precursor for dislocation network formation. The qualitative behavior compares well with the corrugation patterns observed in the systems of flat lattice-mismatched InAs overlayers on infinite GaAs(110) substrates, when misfit dislocation networks are formed in the system. As the aspect ratio increases, the overall upward relaxation in the InAs planes is suppressed, while strong downward movements take place in the mesa systems. This is indicative of compressive stress domain at the center of the mesa with sufficiently large dimensions. The conclusions regarding the mechanism of stress relaxation are supported by the computed hydrostatic stress pattern in the mesa systems of varied geometry. Similar to the displacement fields, the hydrostatic stress in the mesa systems also demonstrates an oscillatory behavior along the $\{110\}$ direction, with the same period of modulations. The stress behaviors, along with those operative for the infinite lattice-mismatched overlayers, provide a comprehensive picture of the stress relaxation pathways in the nanometer-sized overlayer-covered mesa systems. The results support the general picture of lattice-mismatched quantum dot formation on the nonplanar (mesa) substrates.

ACKNOWLEDGMENTS

This work was supported by the U.S. AFOSR through the DURINT program, DOE, and NSF. Simulations were performed using CACS's 256-node Linux cluster and the high-performance computing facilities at the USC.

- ¹A. Madhukar, *Thin Solid Films* **231**, 8 (1993).
- ²*Low-Dimensional Structures Prepared by Epitaxial Growth or Regrowth on Patterned Substrates*, NATO-ASI Series, edited by K. Eberl, P. Petroff, and P. Demeester (Kluwer, Netherlands, 1995), Vol. 279, pp. 19–33.
- ³*Nano-Optoelectronics*, edited by M. Grundmann (Springer, Germany, 2002).
- ⁴D. Srivastava and S. N. Alturi, *Comput. Model. Eng. Sci.* **3**, 531 (2002).
- ⁵A. Konkar, K. C. Rajkumar, Q. Xie, P. Chen, A. Madhukar, H. T. Lin, and D. H. Rich, *J. Cryst. Growth* **150**, 311 (1995).
- ⁶A. Konkar, A. Madhukar, and P. Chen, *Mater. Res. Soc. Symp. Proc.* **380**, 17 (1995).
- ⁷A. Konkar, A. Madhukar, and P. Chen, *Appl. Phys. Lett.* **72**, 220 (1998).
- ⁸A. Konkar, R. Heitz, T. R. Ramachandran, P. Chen, and A. Madhukar, *J. Vac. Sci. Technol. A* **16**, 1334 (1998).
- ⁹R. Zhang, R. Tsui, K. Shiralagi, D. Convey, and H. Goronkin, *Appl. Phys. Lett.* **73**, 505 (1998).
- ¹⁰H. Heidemeyer, C. Muller, and O. G. Schmidt, *J. Cryst. Growth* **261**, 444 (2004).
- ¹¹G. Jin, J. L. Liu, S. G. Thomas, Y. H. Luo, K. L. Wang, and B. Y. Nguyen, *Appl. Phys. Lett.* **75**, 2752 (1999).
- ¹²G. Jin, J. L. Liu, Y. H. Luo, and K. L. Wang, *Thin Solid Films* **380**, 169 (2000).
- ¹³G. Jin, J. Wan, Y. M. Luo, J. L. Liu, and K. L. Wang, *J. Cryst. Growth* **227**, 1100 (2001).
- ¹⁴S. Guha, A. Madhukar, and K. C. Rajkumar, *Appl. Phys. Lett.* **57**, 2110 (1990).
- ¹⁵D. Bimberg, M. Grundmann, and N. N. Ledentsov, *Quantum Dot Heterostructures* (Wiley, UK, 1998).
- ¹⁶S. C. Jain, M. Willander, K. Pinardi, and H. E. Maes, *Phys. Scr., T* **69**, 65 (1997).
- ¹⁷S. C. Jain, H. E. Maes, and K. Pinardi, *Thin Solid Films* **292**, 218 (1997).
- ¹⁸S. C. Jain, A. H. Harker, A. Atkinson, and K. Pinardi, *J. Appl. Phys.* **78**, 1630 (1995).
- ¹⁹K. Pinardi, S. C. Jain, M. Willander, A. Atkinson, H. E. Maes, and R. Van Overstraeten, *J. Appl. Phys.* **84**, 2507 (1998).
- ²⁰S. Christiansen, M. Albrecht, H. P. Strunk, and H. J. Meier, *Appl. Phys. Lett.* **64**, 3617 (1994); **66**, 574 (1995).
- ²¹G. S. Pearson and D. A. Faux, *J. Appl. Phys.* **88**, 730 (2000).
- ²²W. Yu and A. Madhukar, *Proceedings of the 23rd ICPS Conference*, Berlin, Germany, July 1996, edited by M. Scheffler and R. Zimmerman (World Scientific, Singapore, 1996), p. 1309.
- ²³W. Yu and A. Madhukar, *Phys. Rev. Lett.* **79**, 905 (1997); **79**, 4939(E) (1997).
- ²⁴M. A. Makeev and A. Madhukar, *Phys. Rev. Lett.* **86**, 5542 (2001).
- ²⁵M. A. Makeev and A. Madhukar, *Phys. Rev. B* **68**, 195301 (2003).
- ²⁶M. Grundmann, O. Stier, and D. Bimberg, *Phys. Rev. B* **52**, 11969 (1995).
- ²⁷O. Stier, M. Grundmann, and D. Bimberg, *Phys. Rev. B* **59**, 5688 (1999).
- ²⁸A. J. Williamson, L. W. Wang, and A. Zunger, *Phys. Rev. B* **62**, 12963 (2000).
- ²⁹S. J. Sun and Y. C. Chang, *Phys. Rev. B* **62**, 13631 (2000).
- ³⁰H. Jiang and J. Singh, *Phys. Rev. B* **56**, 4696 (1997).
- ³¹C. Pryor, J. Kim, L. W. Wang, A. J. Williamson, and A. Zunger, *J. Appl. Phys.* **83**, 2548 (1998).
- ³²M. E. Bachlechner, A. Omeltchenko, A. Nakano, R. Kalia, P. Vashishta, I. Ebbsjö, A. Madhukar, and P. Messina, *Appl. Phys. Lett.* **72**, 1969 (1998).
- ³³A. Omeltchenko, M. E. Bachlechner, A. Nakano, R. Kalia, P. Vashishta, I. Ebbsjö, A. Madhukar, and P. Messina, *Phys. Rev. Lett.* **84**, 318 (2000).
- ³⁴M. A. Makeev and A. Madhukar, *Appl. Phys. Lett.* **81**, 3789 (2002); M. A. Makeev, W. Yu, and A. Madhukar, *J. Appl. Phys.* **96**, 4429 (2004).
- ³⁵X. Su, R. Kalia, A. Nakano, P. Vashishta, and A. Madhukar, *Appl. Phys. Lett.* **78**, 3717 (2001).
- ³⁶X. Su, R. Kalia, A. Nakano, P. Vashishta, and A. Madhukar, *Appl. Phys. Lett.* **79**, 4577 (2001).
- ³⁷X. Su, R. Kalia, A. Nakano, P. Vashishta, and A. Madhukar, *J. Appl. Phys.* **94**, 6762 (2003).
- ³⁸P. S. Branicio, J. P. Rino, F. Shimojo, R. K. Kalia, A. Nakano, and P. Vashishta, *J. Appl. Phys.* **94**, 3840 (2003).
- ³⁹N. Moll, A. Kley, E. Pihlke, and M. Scheffler, *Phys. Rev. B* **54**, 8844 (1996).
- ⁴⁰P. Vashishta, R. K. Kalia, A. Nakano, W. Li, and I. Ebbsjö, in *Amorphous Insulators and Semiconductors*, NATO Advanced Study Institute Series, edited by M. F. Thorpe and M. I. Mitkova (Kluwer, Dordrecht, 1997), pp. 151–213.
- ⁴¹I. Ebbsjö, R. K. Kalia, A. Nakano, J. P. Rino, and P. Vashishta, *J. Appl. Phys.* **87**, 7708 (2000).
- ⁴²S. Kodyyalam, R. K. Kalia, H. Kikuchi, A. Nakano, F. Shimojo, and P. Vashishta, *Phys. Rev. Lett.* **86**, 55 (2001).
- ⁴³M. Tuckerman, B. J. Berne, and G. J. Martyna, *J. Chem. Phys.* **97**, 1990 (1992).
- ⁴⁴R. J. Hardy, *J. Chem. Phys.* **76**, 622 (1982); V. Vitek and T. Egami, *Phys. Status Solidi B* **144**, 145 (1987).
- ⁴⁵J. F. Lutsko, *J. Appl. Phys.* **65**, 2991 (1989).
- ⁴⁶K. S. Cheung and S. Yip, *J. Appl. Phys.* **70**, 5688 (1991).
- ⁴⁷J. G. Belk, L. J. Sudijono, X. M. Zhang, J. H. Neave, T. S. Jones, and B. A. Joyce, *Phys. Rev. Lett.* **78**, 475 (1997).
- ⁴⁸L. A. Zepeda-Ruiz, D. Maroudas, and W. H. Weinberg, *J. Appl. Phys.* **85**, 3677 (1999).
- ⁴⁹L. A. Zepeda-Ruiz, R. I. Petzel, B. Z. Noshov, W. H. Weinberg, and D. Maroudas, *J. Appl. Phys.* **90**, 2690 (1999).